Journal of Materials Chemistry C

ROYAL SOCIETY OF CHEMISTRY

PAPER

View Article Online
View Journal | View Issue

Check for updates

Cite this: J. Mater. Chem. C, 2025, 13, 6539

Tetrabromobenzene-based molecular alloys – a tool for tailoring the temperature of the thermosalient phase transition†

Teodoro Klaser,[ab] Oskar Stepančić,[ac] Jasminka Popović,[d] Jana Pisk,[e] Luka Pavić,[d] Igor Picek,[f] Dubravka Matković-Čalogović[e] and Željko Skoko*[a]

Received 29th October 2024,
Accepted 11th February 2025

DOI: 10.1039/d4tc04615c

rsc.li/materials-c

A series of molecular alloys of 1,2,4,5-tetrabromobenzene and 1,2,4,5-tetrachlorobenzene with varying compositions were prepared in an attempt to obtain jumping crystals with adjustable temperature of thermosalient phase transition. Molecular alloys were studied with a combination of thermal and structural techniques (DSC, SCXRD, XRPD, hot-stage microscopy). Alloys with a high 1,2,4,5-tetrabromobenzene content (more than 90 wt%) exhibited thermosalient behaviour. Thermosalient alloys exhibited negative uniaxial thermal expansion and colossally large coefficients of thermal expansion (both linear and volumetric), with unit cell parameters increasing proportionally with tetrabromobenzene content. Finally, it was found that the temperature of phase transition increases linearly with the tetrabromobenzene content, from 30.13 °C to 45.33 °C, meaning that the tuning temperature of thermosalient mechanic response was successfully achieved.

Introduction

In the world of materials science, the advent of smart materials has led to significant breakthroughs across various fields, including medicine, robotics, and aerospace. Among these innovative materials, thermosalient materials have emerged as particularly intriguing due to their ability to rapidly and reversibly change shape when exposed to temperature fluctuations. Colloquially known as "jumping crystals", these materials exhibit a remarkable interplay of mechanical and thermal properties with their dynamic structural transformations resulting in dramatic shape changes, ejections, or even explosive movements thus not only making thermosalient crystals an exciting and captivating subject of study, but also a promising option for diverse applications such as actuators, sensors, and devices for energy harvesting.

The discovery of the thermosalient effect can be traced back to 1983, with pioneering work by Etter and Siedle, who reported a peculiar behaviour in (phenylazophenyl)palladium hexafluoroacetylacetonate.[1] Since then, researchers have made significant progress in unravelling the fundamental principles governing the thermosalient phenomenon, elucidating the role of various factors, such as crystallographic symmetry, molecular packing, intermolecular interactions, and energy barriers.[2–56] The exact mechanisms responsible for thermosalient behaviour are still under active investigation. Multiple hypotheses have been proposed, including crystal twinning, conformational changes, and the release of internal stresses. Crystal twinning is particularly relevant for thermosalient organic compounds, where the crystal structure consists of interlocked domains that can shift or rotate with respect to each other. These domain movements can induce significant macroscopic displacements, leading to the observed jumping behaviour.[50,51]

In recent years, advancements in experimental and computational techniques have provided valuable insights into the structural changes occurring during thermosalient events such as high-speed imaging techniques that allowed capturing of rapid movement of thermosalient crystals and enabled a detailed analysis of crystal dynamics.[4,8,20,38,39,45,48,49,51,52,54] Additionally, computational modelling approaches, such as molecular dynamics simulations, complemented experimental

[a] Department of Physics, Faculty of Science, University of Zagreb, Bijenička 32, Zagreb, Croatia. E-mail: zskoko@phy.hr
[b] Department of Physics, University of Trento, Via Sommarive 14, Trento, Italy
[c] Department of Physics, Division of Synchrotron Radiation Research, Lund University, Sweden
[d] Ruđer Bošković Institute, Bijenička 54, Zagreb, Croatia
[e] Department of Chemistry, Faculty of Science, University of Zagreb, Horvatovac 102a, Zagreb, Croatia
[f] Department of Chemistry and Biochemistry, School of Medicine, University of Zagreb, Šalata 3, Zagreb, Croatia

† Electronic supplementary information (ESI) available: DSC curves, got-stage microscopy videos and screenshots, XRD refinements, CIF. CCDC 2393428. For ESI and crystallographic data in CIF or other electronic format see DOI: https://doi.org/10.1039/d4tc04615c

findings by providing an insight to the inherent thermosalient features at the atomistic level.[7,17,43,56–62] Such approaches are of the utmost importance since only the detailed elucidation of underlying mechanisms can enable the design and engineering of innovative materials with exceptional properties and functionalities.

In addition, one of the main goals of research targeted at the thermosalient materials is the ability to modulate the temperature of the thermosalient phase transition, *i.e.* the temperature at which the crystals jump. Being able to change the temperature of the thermosalient phase transition is crucial for tailoring these materials to specific applications, optimizing their performance and safety, enhancing their durability, and ensuring energy-efficient operation. One of the possible ways of achieving this goal is by preparing molecular alloys *i.e.* solid solutions consisting of isostructural compounds, with at least one of them being thermosalient, in different ratios, as shown by Naumov and coauthors.[6] Unlike traditional alloys composed of metal elements, molecular alloys consist of organic molecules, small molecules, or even polymers, which can interact through various intermolecular forces like van der Waals forces, hydrogen bonds, π–π interactions, or charge-transfer complexes. Molecular alloys consist of different types of molecules mixed uniformly at the molecular level, often resulting in a single, homogeneous phase. This uniform mixing is critical to their properties and distinguishes them from mixtures or composites, where components are phase-separated. The properties of molecular alloys can be tuned by adjusting the ratio, size, shape, and chemical nature of the constituent molecules. This tunability is one of the most appealing aspects, allowing for a wide range of optical, electronic, thermal, and mechanical properties. Some of the main advantages of molecular alloys are their customization, scalability, versatility and simplicity of preparation.

For this purpose, a series of molecular alloys composed of 1,2,4,5-tetrabromobenzene (TBB) and 1,2,4,5-tetrachlorobenzene (TCB) were prepared in various ratios. These two compounds were selected due to their isostructural nature and their status as well-known and extensively studied thermosalient materials.[63–66] Thermosalience of TBB was first discovered by Davey[50] in 2000 who found that the compound crystallizes in two polymorphic forms: the β-phase, which is stable at room temperature (RT), and the high-temperature (HT) γ-phase, which is stable above 46 °C. The phase transition between β and γ is characterized by the crystals "jumping". Further investigations of thermosalient effect in this compound were conducted in detail by Naumov *et al.*[43,44,51,67,68] who also demonstrated the first practical application of thermosalient crystals, using TBB as an active material in a novel hybrid material for electrical fuse links.[67] Unlike TBB which exhibits thermosalient phase transition at temperature slightly above room temperature, TCB undergoes this transition well below room temperature, specifically between −109 °C and −96 °C.[27,69] Like TBB, the reversible thermosalient effect in TCB is driven by subtle changes in the molecular orientation of its sheets.[27]

The motivation for this study was to find a simple and effective way to tune the temperature of the thermosalient phase transition. TBB was chosen because the temperature of thermosalient transition is approximately 46 °C which is close to the human body temperature. This study shows it is possible to bring it down to the actual human body temperature, which might be particularly valuable for biomedical and wearable technology applications, by the utilization of TBB–TCB molecular alloys having the TBB content between 94 and 95 wt%.

Results and discussion

Thermal analysis and hot stage microscopy

DSC measurements were conducted on as-prepared samples to examine phase transitions in molecular alloys TBB–TCB with nominal content of TBB 76, 80, 84, 88, 90, 92, 94, 95, 96, 98, 99, 100 wt%, which corresponds to 63, 69, 74, 80, 83, 86, 90, 91, 93, 96, 98, 100 mol%. The actual content of TBB, as determined by EDS, amounts to 72, 77, 81, 85, 88, 90, 92, 94, 95, 98, 99, 100 wt%, which corresponds to 59, 65, 70, 76, 80, 83, 86, 90, 91, 96, 98, 100 mol% (Table S1, ESI†). Samples in this work are labeled according to their nominal composition. Multiple heating and cooling cycles between 20 °C and 150 °C were performed to ensure the reproducibility of the results. No thermal events were observed, neither during heating nor cooling, for samples containing 90 wt% and lower of TBB. Contrary to that, as shown in Fig. 1(a) and Fig. S2 (ESI†), for all samples with 92 wt% TBB and higher a single endothermic peak was detected during heating and an exothermic peak during the cooling. DSC peaks are uneven and saw-like which is consistent with other thermosalient materials.[8,54] As it can be seen from Fig. 1(a), the temperature of phase transition decreases from 45.33 °C for the pure TBB sample to 30.13 °C for the sample containing 92 wt% TBB. That shows that the temperature of the phase

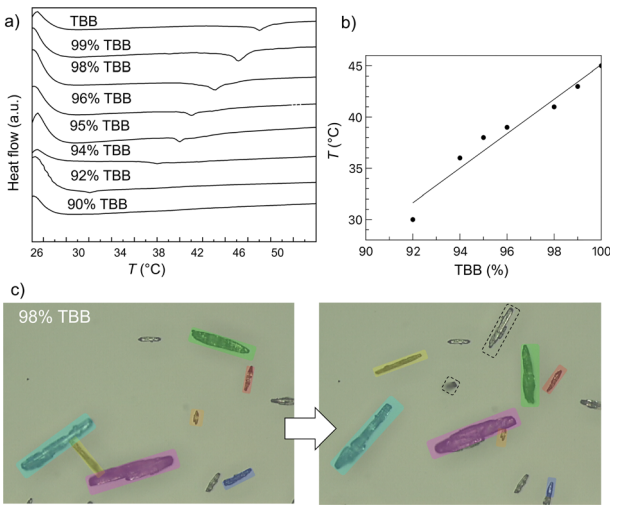

Fig. 1 (a) DSC curves of the samples with 90, 92, 94, 95, 96, 98, 99 and 100 wt% of TBB during the heating run, (b) linear relation between the phase transition temperature and TBB content during heating run, (c) hot-stage microscopy screenshots prior and after the thermosalient phase transition for sample with 98 wt% TBB (dashed lines represent crystals that have jumped into the frame; crystals that jumped and remained inside the frame are coloured in blue, yellow, pink, green, orange and purple).

transition can be varied in the interval of 15 °C by simply varying the composition of the molecular alloy by up to 8 wt%. DSC curves show almost linear relationship between the temperature of the phase transition and the content of TBB in the molecular alloys (Fig. 1(b)). Hot-stage microscopy screenshots prior and after the thermosalient phase transition for the sample with 98 wt% TBB are shown in the Fig. 1(c).

The enthalpies of phase transitions for the samples with TBB content of 92, 94, 95, 96, 98, 99 and 100 wt% acquired from the DSC curves amount to 0.14(1), 0.15(1), 0.18(1), 0.21(1), 0.42(1), 0.53(1) and 0.58(1) J g^{-1} respectively. It should be noted that although it is onerous to calculate precise enthalpies, due to the irregular and uneven nature of the DSC profiles of thermosalient phase transitions, it is obvious that they decrease as the TBB content is reduced. During cooling runs, temperature hysteresis is observed which is typical for thermosalient materials.[7,11,22,48,49] The hysteresis was approximately 10 °C for pure TBB and it decreased with the reduction of TBB content amounting to 5 °C for the alloy with 92 wt% TBB. Similar hysteresis behaviour for a different kind of thermosalient molecular alloys is found in the study conducted by Naumov *et al.*[6]

The thermosalient nature of prepared molecular alloys was investigated and confirmed by means of hot-stage microscopy (Fig. S3 and Videos S1–S4, ESI†). The thermosalient effect was observed using a hot-stage microscope for all the samples with the TBB content 92% and higher, where crystals exhibited sudden, dynamic movements, or "jumps", when heated or cooled. The crystals were jumping within a narrow temperature range of approximately ±3 °C around their phase transition temperature. This temperature interval remained consistent regardless of the specific sample composition. However, the intensity of the crystal jumps became more pronounced and energetic as the TBB content in the samples increased, indicating a correlation between TBB concentration and the energy of the thermosalient effect. This aligns with the fact that the calculated enthalpies of the phase transitions increase as the TBB content in the samples gets higher.

XRD structural analysis

After the confirmation of the thermosalient nature of phase transitions by the hot-stage microscopy, detailed *in situ* high temperature X-ray powder diffraction (HT-XRPD) study of

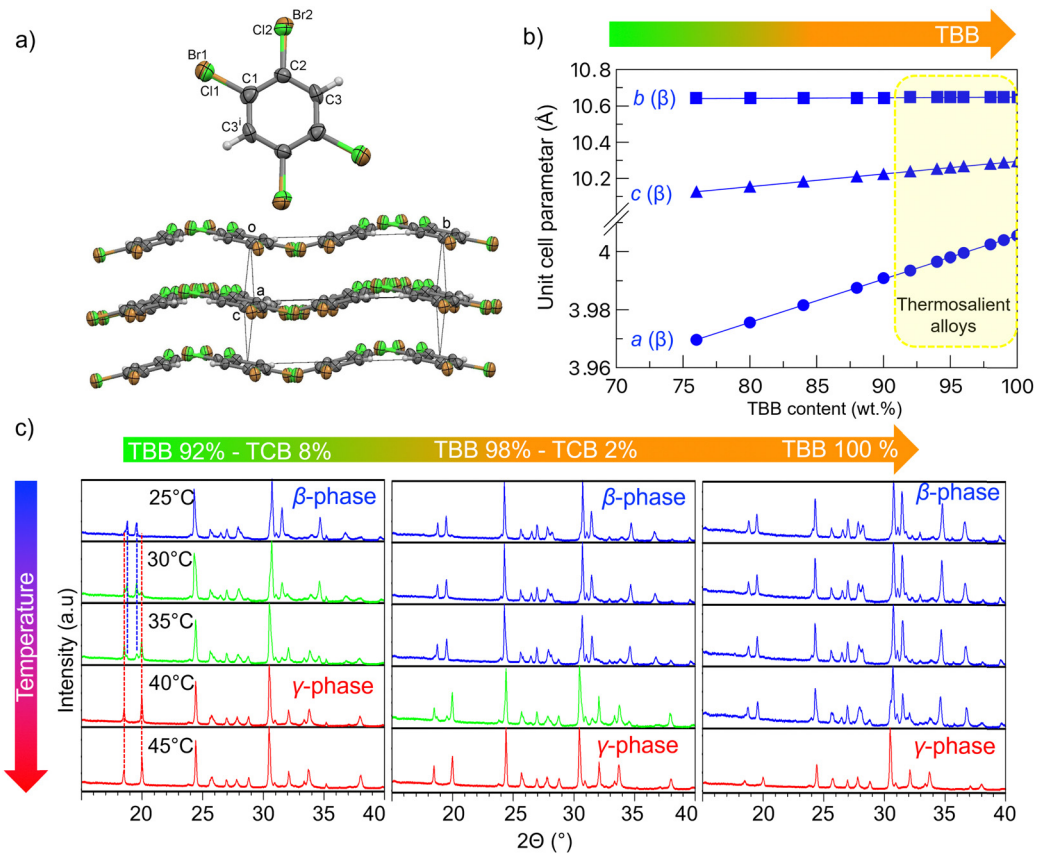

Fig. 2 (a) Molecular structure and crystal pacing of molecular alloy containing 98 wt% of TBB (b) Linear increase of unit-cell parameters for series of molecular alloys in the whole ranges from 76 to 99 wt% of TBB with the increase in TBB content. TBB content of alloys exhibiting thermosalient behaviour is highlighted in yellow. The error bars are smaller than the symbol sizes. (c) XRPD patterns of TBB–TCB molecular alloys with different compositions at selected temperatures during heating from RT to 45 °C. XRPD patterns of molecular alloy with 92 wt% TBB is shown at the left, 98 wt% TBB in the middle and pure TBB at the right-hand side. Patterns that contain low temperature β-phase are shown in blue, patterns where both β- and γ-phase are in coexistence are given in green while the patterns consisting only of high temperature γ-phase are shown in red. The difference between β- and γ-phase is most clearly seen in the 2θ range ≈ 18–20° by following vertical red and blue dashed lines as a guideline for the eye.

crystal structure was performed for all the samples exhibiting thermosalient effect (content of TBB of 92 wt% and higher). XRPD patterns were collected during heating in the temperature interval from RT to 60 °C followed by cooling runs back to room temperature. Fig. 2(a) shows the molecular structure and crystal packing of the molecular alloy with 98 wt% TBB and 2 wt% TCB as determined by single crystal X-ray diffraction. Structure determination revealed that the molecular alloy with 98 wt% TBB indeed has formed and it exhibits, as expected, the structure as its dominant component *i.e.* β-phase TBB. TBB molecules are randomly replaced by TCB molecules in the crystal structure. The molecules are interconnected into puckered sheets by halogen bonds and C–H···Br/Cl weak hydrogen bonds (Fig. 2(a)). In TBB the Br···Br contacts are 3.619 and 3.923 Å,[50] whereas in $C_6H_2Br_{3.86}Cl_{0.14}$ they amount to 3.629(2) and 3.901(2) Å. The Cl···Br contacts are longer and are in the range 3.656(5) to 4.029(5) Å. Crystal data and structure refinement details for the crystal with 98 wt% TBB, selected bond lengths, angles and torsion angles are given in Tables S2–S5 (ESI†), respectively. Successful formation of molecular alloys in the whole ranges from 72 to 99 wt% of TBB is obvious from the linear increase of the unit-cell parameters with the increase in TBB content, as shown in Fig. 2(b). Fig. 2(c) shows XRPD patterns collected during heating from RT to 45 °C, recorded at intervals of 5 °C, for three representative molecular alloys: 92 wt% TBB – 8 wt% TCB, 98 wt% TBB – 2 wt% TCB and pure TBB. These compositions were selected as they represent the boundary conditions in which TBB–TCB molecular alloys exhibit the thermosalient effect, alongside pure TBB. At room temperature all samples contain solely the low temperature β-phase. Phase purity of samples at RT, *i.e.* absence of diffraction lines that would correspond to TCB is particularly important to notice since that confirms a successful formation of molecular alloys within the studied TBB:TCB range. Consistent with the DSC results, sample with 92 wt% TBB undergoes the thermosalient transformation to the high temperature γ-phase at 30 °C.

In this sample, the β- and γ-phases coexist at 30 °C and 35 °C. At higher temperatures, 40 °C and above, the sample is composed entirely of the high temperature γ-phase. Similarly, the sample with 98 wt% TBB consists of low temperature β-phase up to (and including) 35 °C. Thermosalient phase transition from β- to γ-phase occurs at 40 °C where the two phases are in coexistence, and the sample consists of pure high temperature γ-phase at 45 °C and higher. Pure TBB sample contains low temperature β-phase up to (and including) 40 °C after which it transforms into γ-phase and is fully transformed at 45 °C. All the other thermosalient samples with different compositions exhibit similar behaviour fully consistent with thermal measurements.

Thermal expansion of the unit cell parameters of the samples 92 wt% TBB – 8 wt% TCB, 98 wt% TBB – 2 wt% TCB and pure TBB is shown in Fig. 3(a), whereas the thermal expansivity indicatrix are shown in Fig. 3(b). The relationship between the principal axes and the crystallographic axes, along with the coefficients of linear thermal expansion along principal axes is shown in Table S6 (ESI†). The unit-cell parameters of β- and γ-phases have been determined by the Le Bail fitting; selected refinements are shown in Fig. S3 (ESI†). Unit-cell parameters were also determined from the data collected during second heating run and were found to be within the standard deviation range compared to the values obtained during the first heating and cooling runs. Thermosalient TBB–TCB molecular alloys exhibit colossal values of thermal expansion. Linear thermal expansion coefficients of molecular organic crystals typically are in the range $0 \times 10^{-6} < \alpha < 20 \times 10^{-6}$ K^{-1}, but the values in this system are much higher. Along the *a*-direction, the values of thermal expansion coefficient lie between 172–226 $\times 10^{-6}$ K^{-1} while the values along the *b*-direction are in the range of 243–389 K^{-1}, making them 10–20 times larger than the usual largest values. Furthermore, these molecular alloys exhibit uniaxial negative thermal expansion, quite common for the thermosalient materials, along the *c*-axis, in the range of (−155) to (−326) $\times 10^{-6}$ K^{-1}, which is also strikingly high. The overall volume thermal expansion of the crystals is also extremely high, amounting to 121–250 $\times 10^{-6}$ K^{-1} for the low temperature β-phase and colossal 266–326 $\times 10^{-6}$ K^{-1} for high temperature γ-phase. These values are in accordance with the results for pure TBB obtained by Zakharov *et al.*[47] No systematic difference in the values was observed between the samples of different compositions or between low temperature β- and high temperature γ-phase. Only a handful of materials with such high thermal expansion coefficients can be found in the literature. Mostly they exhibit positive thermal expansion[41,70–78] but also negative thermal expansion.[7,8,48,72,79–85] Negative uniaxial thermal expansion which is present in TBB–TBC molecular alloys is also quite often characteristic in thermosalient materials, as is a discontinuation of the cell dimension variation at the phase transition. This discontinuation is approximately 0.5% for *a*-direction, independent of the molecular alloy composition. It increases from 2% for sample with 92 wt% TBB to 3% for pure TBB in *b*-direction. Similarly, the increment from −2% to −3% is also observed in *c*-direction for these samples. It is obvious that the discontinuation parallel to *b*- and *c*-directions increases with the TBB content.

First attempt at systematic explanation for the thermosalient effect in TBB was given by Davey *et al.*[50] stating that hydrogen–bromide and bromide–bromide interactions arising from the nonuniformity of the electrostatic potential on the bromide atom thus causing TBB molecules to arrange in the layered structure and provoking order–disorder thermosalient phase transition. The mechanism was further elucidated by Naumov *et al.*[43,51,68] who found that the thermosalient phase transition in this system is displacive-type and associated with the softening of the lowest transverse acoustic mode on approaching the phase transition which serves as a gateway to incite the phase transition and a starting point for storing the mechanical strain which causes crystals to jump. Softening of the crystal lattice on temperatures near the phase transition was also confirmed by Zakharov *et al.*[47] Also, like most other thermosalient materials, the system TBB–TCB also exhibits negative thermal expansion. This unusual property contributes to the build-up of the anisotropic crystal lattice strain, which, when

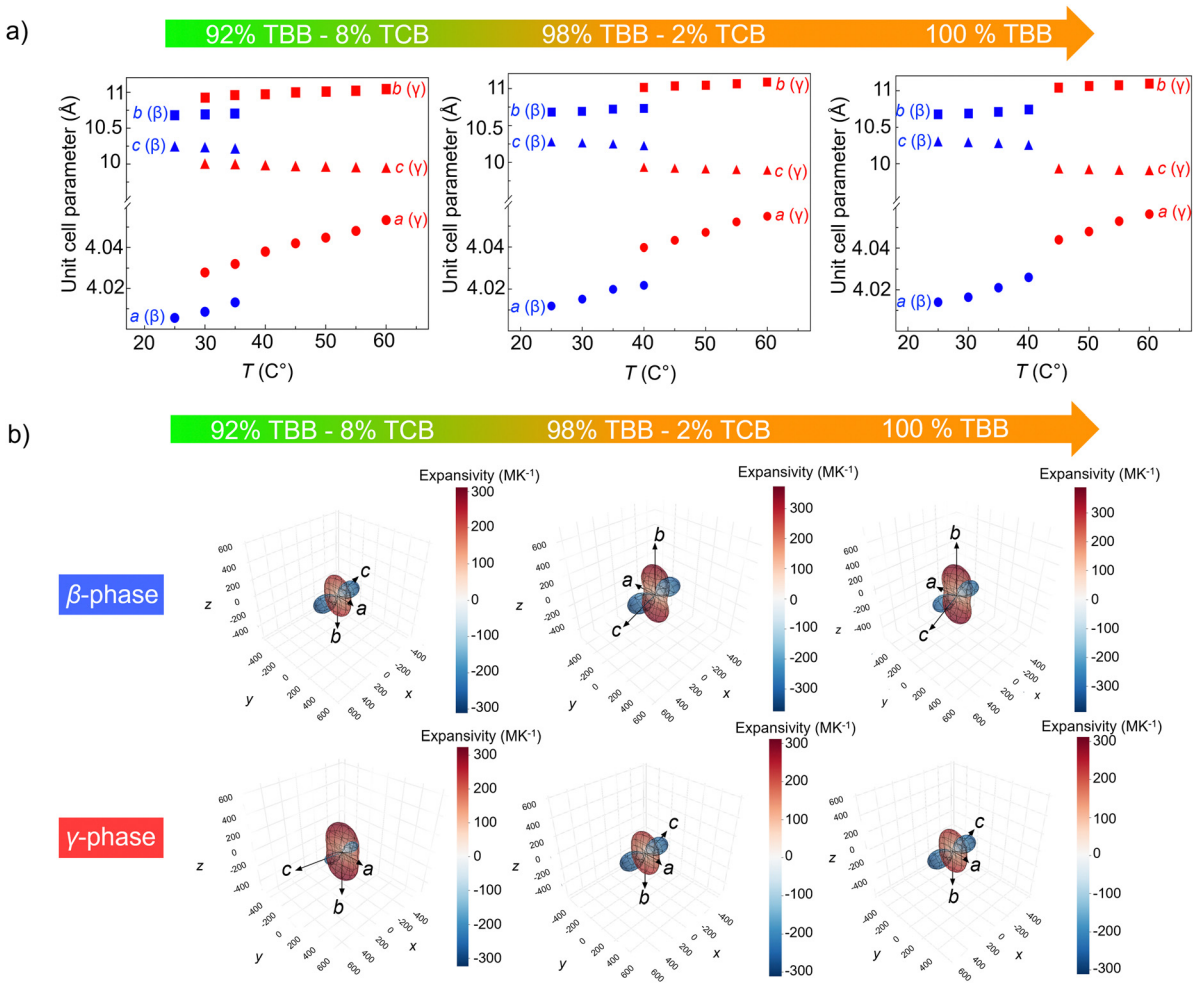

Fig. 3 (a) Temperature dependence of the unit-cell parameters of the low temperature β- and high temperature γ-phase for the molecular alloys containing 92, 98 and 100 wt% of TBB. (b) Thermal expansivity indicatrix of low temperature β- and high temperature γ-phase for the molecular alloys containing 92, 98 and 100 wt% of TBB.

released results in the mechanical motion of the crystals. Considering that TTB–TCB alloys exhibit the same structure as β-phase of TBB, it is reasonable to assume that the mechanism responsible for thermosalient phenomenon in TBB–TCB molecular alloys and pure TBB is similar while chlorine content in molecular alloy provides an effective tool for tailoring the temperature of the phase transition.

Experimental

Chemicals and materials

Commercially obtained 1,2,4,5-tetrabromobenzene (Sigma-Aldrich, purity 97.0%) and 1,2,4,5-tetrachlorobenzene (Tokyo Chemical Industry, purity >99.0%) were mixed in different weight ratios (100 : 0, 99 : 1, 98 : 2, 96 : 4, 95 : 5, 94 : 6, 92 : 8, 90 : 10, 88 : 12, 84 : 16, 80 : 20, 76 : 24), then dissolved in diethyl ether (Panreac, purity ≥99.7%) and left to crystallize by the slow evaporation at room temperature. This resulted in the crystallization of needle-like crystals of $TBB_xTCB_{(1-x)}$ molecular alloy suitable for single crystal X-ray diffraction. The samples for X-ray powder diffraction were obtained by careful grinding of the crystals in an agate mortar.

The actual composition of the prepared alloys was determined by energy-dispersive X-ray spectroscopy (EDS) and is given in Table S1 (ESI†). Samples in this work are labeled according to their nominal composition.

Single crystal X-ray diffraction (SCXRD)

Single crystal XRD measurements were collected from a single crystal with 98 wt% TBB, glued to a thin glass fiber, on an Oxford Diffraction Xcalibur Sapphire3 diffractometer with graphite-monochromator using MoK_α radiation (λ = 0.71073 Å). The crystal was kept at 293(2) K during data collection. Data collection and reduction was performed using the CrysAlis software package (Version 1.171.39.46, Rigaku Oxford Diffraction, 2018). Empirical absorption correction was done using spherical harmonics. By using Olex2,[86] the structure was solved with the SHELXT program[87] using intrinsic phasing and refined with SHELXL using least-squares minimization based on F^2.[87] The C–Cl bond length was restrained to 1.722 Å, according to the

distance from the room temperature of TCB structure reported under Refcode TCLBEN08. Atoms Br and Cl were restrained to have the same U_{ij} components. The hydrogen atom was positioned in the calculated position with $U_{iso}(H) = 1.2U_{eq}(C)$ using the riding model with C–H = 0.93 Å. Occupancies of Br and Cl were fixed at 0.964 and 0.036, respectively. Drawings of the structure were prepared by MERCURY.[88]

X-ray powder diffraction (XRPD)

XRPD patterns were recorded by *in situ* HT variable temperature (VT) XRPD using Bruker D8 Discover diffractometer equipped with a LYNXEYE XE-T detector with Ni filter using monochromatic CuKα_1 radiation (λ = 1.54060 Å) and an Anton Paar High-Temperature Oven-Chamber HTK1200N with CCU 1000 control unit. The scans were recorded in 2θ range 10–60° with a step of 0.02°, measuring time 1 s per step, with a 2.5° Soller slit and fixed slit at 0.4 mm. The slit opening in front of the detector was 6.5 mm, and the detector opening was 1.3°, resulting in an integrating time per step of 125 s. Data were collected in the temperature range 25–60 °C. Heating rate was 5 °C min^{-1} and the heating was stopped every 5 °C (25, 30, 35, 40, 45, 50, 55, 60 °C), held for 15 min for stabilization of the sample after which the recordings were made. Structural analysis was conducted using HighScore X'pert Plus software (Version 4.5, March 2016). Thermal expansion coefficients were calculated from the refined unit cell parameters obtained from variable temperature diffraction data. Linear axial thermal expansion coefficients along the principal axes were calculated using the PASCal software.[89]

Thermal analysis

Differential scanning calorimetry (DSC) measurements were carried out using a Mettler-Toledo DSC823e calorimeter and analyzed with Mettler STARe 9.01 software. The measurements were performed in aluminum crucibles, in the nitrogen atmosphere, with the heating rate 5 °C min^{-1} in the temperature range between 20 °C and 150 °C.

Hot-stage microscopy

Mechanical behavior during heating/cooling was examined and recorded using Nikon Eclipse LV150NL (Nikon) optical microscope equipped with a Linkam THMS600 hot-stage and OPTOCAM-II color camera with a resolution of 1600 × 1200 pixels. Crystal behavior was monitored in the temperature interval from room temperature to the melting point (~180 °C).

Energy-dispersive X-ray spectroscopy (EDS)

The Axia ChemiSEM Scanning Electron Microscope (Thermo Fisher Scientific) with an integrated energy-dispersive X-ray analyzer was used for elemental analysis.

Conclusions

This study shows that TBB and TCB form molecular alloys in a wide range with unit cell parameters increasing linearly with the TBB content. The alloys rich in TBB (with concentration of TBB higher than 90%) exhibit thermosalient behaviour similar in nature to that of pure TBB. The temperature of the thermosalient phase transition in these alloys increases linearly with the TBB content. The transition temperature can easily be finely tuned within a 15 °C range by varying the TBB content, highlighting the versatility of these alloys. These findings underscore the potential of TBB–TCB molecular alloys for applications that leverage their remarkable thermal response and expand the understanding of phase behaviour in thermosalient systems. One of the key challenges in the practical application of thermosalient materials is the fixed nature of their phase transition temperatures. This study demonstrates that by simply creating thermosalient molecular alloys, the transition temperature can be effectively adjusted, bringing us a step closer to the commercial utilization of this intriguing yet not fully understood phenomenon.

Author contributions

Ž. S. designed and conceptualized the whole study, analysed and interpreted results and wrote the first version of the manuscript. I. P. prepared the samples. T. K. and O. S. conducted *in situ* XRD and hot-stage microscopy measurements and provided the qualitative analysis. D. M.-Č. collected SCXRD data and conducted structure determination. T. K., J. Po. and Ž. S. conducted detailed structural analysis of *in situ* HT-XRPD data including refinements of unit-cell parameters and the interpretation of thermal expansion. L. P. and J. Pi. conducted and interpreted the DSC study. All authors contributed to the final version of the text.

Data availability

The data supporting this article are included as part of the ESI.† CCDC 2393428 contains the supplementary crystallographic data for $C_6H_2Br_{3.86}Cl_{0.14}$.

Conflicts of interest

There are no conflicts to declare.

Acknowledgements

Ž. S., J. Pi. and D. M.-Č. acknowledge the support of projects CeNIKS (grant no. KK.01.1.1.02.0013) and CIuK (grant KK.01.1.1.02.0016), respectively, co-financed by the Croatian government and the European Union through the European Regional Development Fund, Competitiveness and Cohesion Operational Programme. Ž. S. acknowledges the support of project ''Tuning of the temperature of thermosalient phase transitions'' financed by the Croatian Academy of Sciences and Arts Foundation.

Notes and references

1 M. C. Etter and A. R. Siedle, *J. Am. Chem. Soc.*, 1983, **105**, 641–643.
2 T. Steiner, W. Hinrichs, W. Saenger and R. Gigg, *Acta Crystallogr., Sect. B: Struct. Sci.*, 1993, **49**, 708–718.
3 K. Takazawa, J. Inoue and Y. Matsushita, *Small*, 2022, **18**, 2204500–2204508.
4 M. K. Panda, T. Runčevski, S. Chandra Sahoo, A. A. Belik, N. K. Nath, R. E. Dinnebier and P. Naumov, *Nat. Commun.*, 2014, **5**, 4811.
5 S. Ohtani, M. Gon, K. Tanaka and Y. Chujo, *Chem. – Eur. J.*, 2017, **23**, 11827–11833.
6 E. Nauha, P. Naumov and M. Lusi, *CrystEngComm*, 2016, **18**, 4699–4703.
7 I. Lončarić, J. Popović, V. Despoja, S. Burazer, I. Grgičević, D. Popović and Ž. Skoko, *Cryst. Growth Des.*, 2017, **17**, 4445–4453.
8 M. K. Panda, R. Centore, M. Causà, A. Tuzi, F. Borbone and P. Naumov, *Sci. Rep.*, 2016, **6**, 29610.
9 T. Takeda and T. Akutagawa, *Chem. – Eur. J.*, 2016, **22**, 7763–7770.
10 Y. Shibuya, Y. Itoh and T. Aida, *Chem. – Asian J.*, 2017, **12**, 811–815.
11 Ž. Skoko, S. Zamir, P. Naumov and J. Bernstein, *J. Am. Chem. Soc.*, 2010, **132**, 14191–14202.
12 T. Seki, T. Mashimo and H. Ito, *Chem. Lett.*, 2020, **49**, 174–177.
13 J. Mahmoud Halabi, I. Séguy, L. Salvagnac, T. Leïchlé, D. Saya, F. Mathieu, B. Duployer, D. P. Karothu, L. Nicu and P. Naumov, *Cell Rep. Phys. Sci.*, 2022, **3**, 101133.
14 D. P. Karothu, J. Mahmoud Halabi, L. Li, A. Colin-Molina, B. Rodríguez-Molina and P. Naumov, *Adv. Mater.*, 2020, **32**, 1906216–1906226.
15 Y. Miura, T. Takeda, N. Yoshioka and T. Akutagawa, *Cryst. Growth Des.*, 2022, **22**, 5904–5911.
16 G. C. George, S. J. Kruse, T. Z. Forbes and K. M. Hutchins, *Chem. Commun.*, 2024, **60**, 7697–7700.
17 S.-W. An, T. Bo, H.-M. Wang, L. Meng, X. Zhang, Z.-W. Huang, K.-Q. Hu, W.-Q. Shi and L. Mei, *Cryst. Growth Des.*, 2024, **24**, 4357–4367.
18 Q. Di, M. B. Al-Handawi, L. Li, P. Naumov and H. Zhang, *Angew. Chem., Int. Ed.*, 2024, **63**, e202403914–e202403921.
19 D. Manoharan, S. Ranjan, F. Emmerling, B. Bhattacharya, S. Takamizawa and S. Ghosh, *J. Mater. Chem. C*, 2024, **12**, 2515–2525.
20 W. Wu, K. Chen, H. Yu, J. Zhu, Y. Feng, J. Wang, X. Huang, L. Li, H. Hao, T. Wang, N. Wang and P. Naumov, *Chem. Sci.*, 2024, **15**, 9287–9297.
21 P. Naumov, D. P. Karothu, E. Ahmed, L. Catalano, P. Commins, J. Mahmoud Halabi, M. B. Al-Handawi and L. Li, *J. Am. Chem. Soc.*, 2020, **142**, 13256–13272.
22 Y. Duan, S. Semin, P. Tinnemans, J. Xu and T. Rasing, *Small*, 2021, **17**, 2006757–2006763.
23 B. B. Rath, G. Gallo, R. E. Dinnebier and J. J. Vittal, *J. Am. Chem. Soc.*, 2021, **143**, 2088–2096.
24 L. Mei, S. An, K. Hu, L. Wang, J. Yu, Z. Huang, X. Kong, C. Xia, Z. Chai and W. Shi, *Angew. Chem., Int. Ed.*, 2020, **59**, 16061–16068.
25 K. Omoto, T. Nakae, M. Nishio, Y. Yamanoi, H. Kasai, E. Nishibori, T. Mashimo, T. Seki, H. Ito, K. Nakamura, N. Kobayashi, N. Nakayama, H. Goto and H. Nishihara, *J. Am. Chem. Soc.*, 2020, **142**, 12651–12657.
26 Y. Takahashi, T. Kondo, S. Yokokura, M. Takehisa, J. Harada, T. Inabe, M. M. Matsushita and K. Awaga, *Cryst. Growth Des.*, 2020, **20**, 4758–4763.
27 D. P. Karothu and P. Naumov, *Isr. J. Chem.*, 2021, **61**, 557–562.
28 Y. Kikuchi and S. Matsumoto, *CrystEngComm*, 2021, **23**, 5882–5890.
29 B. B. Rath, M. Gupta and J. J. Vittal, *Chem. Mater.*, 2022, **34**, 178–185.
30 R. Chinnasamy, B. Munjal, R. Suryanarayanan, A. M. P. Peedikakkal, M. K. Mishra and S. Ghosh, *Cryst. Growth Des.*, 2022, **22**, 615–624.
31 Y. Zheng, X. Jia, K. Li, J. Xu and X. H. Bu, *Adv. Energy Mater.*, 2022, **12**, 202100324.
32 S. Masuda, S. Kusumoto, M. Okamura, S. Hikichi, R. Tokunaga, S. Hayami, Y. Kim and Y. Koide, *Dalton Trans.*, 2023, **52**, 10531–10536.
33 F. F. Martins, A. Joseph, H. P. Diogo, M. E. Minas da Piedade, L. P. Ferreira, M. D. Carvalho, S. Barroso, M. J. Romão, M. J. Calhorda and P. N. Martinho, *Eur. J. Inorg. Chem.*, 2018, 2976–2983.
34 T. Klaser, J. Popović, J. A. Fernandes, S. C. Tarantino, M. Zema and Ž. Skoko, *Crystals*, 2018, **8**, 301.
35 A. Colin-Molina, D. P. Karothu, M. J. Jellen, R. A. Toscano, M. A. Garcia-Garibay, P. Naumov and B. Rodríguez-Molina, *Matter*, 2019, **1**, 1033–1046.
36 Y. Kamo, I. Nagaya, R. Sugino and H. Hagiwara, *Chem. Lett.*, 2019, **48**, 1077–1080.
37 T. Seki, T. Mashimo and H. Ito, *Chem. Sci.*, 2019, **10**, 4185–4191.
38 A. Khalil, D. P. Karothu and P. Naumov, *J. Am. Chem. Soc.*, 2019, **141**, 3371–3375.
39 M. I. Tamboli, D. P. Karothu, M. S. Shashidhar, R. G. Gonnade and P. Naumov, *Chem. – Eur. J.*, 2018, **24**, 4133–4139.
40 H. Rawat, R. Samanta, B. Bhattacharya, S. Deolka, A. Dutta, S. Dey, K. B. Raju and C. M. Reddy, *Cryst. Growth Des.*, 2018, **18**, 2918–2923.
41 L. O. Alimi, D. P. van Heerden, P. Lama, V. J. Smith and L. J. Barbour, *Chem. Commun.*, 2018, **54**, 6208–6211.
42 H.-S. So, T. Minami, T. Jindo and S. Matsumoto, *CrystEngComm*, 2018, **20**, 5317–5320.
43 A. J. Zaczek, L. Catalano, P. Naumov and T. M. Korter, *Chem. Sci.*, 2019, **10**, 1332–1341.
44 A. Khalil, C. T. Hu and P. Naumov, *CrystEngComm*, 2018, **20**, 636–642.
45 S. C. Sahoo, N. K. Nath, L. Zhang, M. H. Semreen, T. H. Al-Tel and P. Naumov, *RSC Adv.*, 2014, **4**, 7640.
46 S. Ghosh, M. K. Mishra, S. Ganguly and G. R. Desiraju, *J. Am. Chem. Soc.*, 2015, **137**, 9912.

47 B. A. Zakharov, A. A. L. Michalchuk, C. A. Morrison and E. V. Boldyreva, *Phys. Chem. Chem. Phys.*, 2018, **20**, 8523–8532.
48 M. K. Panda, T. Runčevski, A. Husain, R. E. Dinnebier and P. Naumov, *J. Am. Chem. Soc.*, 2015, **137**, 1895–1902.
49 D. P. Karothu, J. Weston, I. T. Desta and P. Naumov, *J. Am. Chem. Soc.*, 2016, **138**, 13298–13306.
50 H. F. Lieberman, R. J. Davey and D. M. T. Newsham, *Chem. Mater.*, 2000, **12**, 490–494.
51 S. C. Sahoo, S. B. Sinha, M. S. R. N. Kiran, U. Ramamurty, A. F. Dericioglu, C. M. Reddy and P. Naumov, *J. Am. Chem. Soc.*, 2013, **135**, 13843–13850.
52 P. Commins, I. T. Desta, D. P. Karothu, M. K. Panda and P. Naumov, *Chem. Commun.*, 2016, **52**, 13941–13954.
53 M. K. Panda, M. Etter, R. E. Dinnebier and P. Naumov, *Angew. Chem., Int. Ed.*, 2017, **56**, 8104–8109.
54 S. C. Sahoo, M. K. Panda, N. K. Nath and P. Naumov, *J. Am. Chem. Soc.*, 2013, **135**, 12241–12251.
55 E. R. Engel, V. J. Smith, C. X. Bezuidenhout and L. J. Barbour, *Chem. Mater.*, 2016, **28**, 5073–5079.
56 M. Dharmarwardana, S. Pakhira, R. P. Welch, C. Caicedo-Narvaez, M. A. Luzuriaga, B. S. Arimilli, G. T. McCandless, B. Fahimi, J. L. Mendoza-Cortes and J. J. Gassensmith, *J. Am. Chem. Soc.*, 2021, **143**, 5951–5957.
57 T. Takeda, M. Ozawa and T. Akutagawa, *Angew. Chem., Int. Ed.*, 2019, **58**, 10345–10352.
58 Y. Duan, S. Semin, P. Tinnemans, H. Cuppen, J. Xu and T. Rasing, *Nat. Commun.*, 2019, **10**, 4573.
59 D. P. Karothu, R. Ferreira, G. Dushaq, E. Ahmed, L. Catalano, J. M. Halabi, Z. Alhaddad, I. Tahir, L. Li, S. Mohamed, M. Rasras and P. Naumov, *Nat. Commun.*, 2022, **13**, 2823.
60 J. Anwar, S. C. Tuble and J. Kendrick, *J. Am. Chem. Soc.*, 2007, **129**, 2542–2547.
61 M. Singh, V. G. Abhijitha, B. R. K. Nanda, D. Pareek, S. Nath, S. Anwar, A. Kumar, P. K. Nanda and S. C. Sahoo, *Chem. Eng. J.*, 2023, **464**, 142665.
62 S. K. Park, H. Sun, H. Chung, B. B. Patel, F. Zhang, D. W. Davies, T. J. Woods, K. Zhao and Y. Diao, *Angew. Chem., Int. Ed.*, 2020, **59**, 13004–13012.
63 F. Michaud, P. Negrier, Y. Haget, J.-M. Leger, C. Courseille, M. A. Cuevas Diarte and H. A. J. Oonk, *J. Appl. Crystallogr.*, 1997, **30**, 1152–1155.
64 D. Mondieig, M. A. Cuevas-Diarte and Y. Haget, *J. Therm. Anal.*, 1989, **35**, 2491–2500.
65 M. J. van Genderren, D. Mondieig, Y. Haget, Ma. C. Diarte and H. A. J. Oonk, *CALPHAD: Comput. Coupling Phase Diagrams Thermochem.*, 1992, **16**, 1–12.
66 D. Mondieig, J. R. Housty, Y. Haget, M. A. Cuevas-Diarte and H. A. J. Oonk, *Thermochim. Acta*, 1991, **177**, 169–186.
67 A. Khalil, E. Ahmed and P. Naumov, *Chem. Commun.*, 2017, **53**, 1–4.
68 J.-H. Ko, K.-S. Lee, S. Chandra Sahoo and P. Naumov, *Solid State Commun.*, 2013, **173**, 46–50.
69 S. A. Barnett, C. K. Broder, K. Shankland, W. I. F. David, R. M. Ibberson and D. A. Tocher, *Acta Crystallogr., Sect. B: Struct. Sci.*, 2006, **62**, 287–295.
70 S. Haas, B. Batlogg, C. Besnard, M. Schiltz, C. Kloc and T. Siegrist, *Phys. Rev. B: Condens. Matter Mater. Phys.*, 2007, **76**, 205203.
71 W. Cai, J. He, W. Li and A. Katrusiak, *J. Mater. Chem. C*, 2014, **2**, 6471–6476.
72 A. L. Goodwin, M. Calleja, M. J. Conterio, M. T. Dove, J. S. O. Evans, D. A. Keen, L. Peters and M. G. Tucker, *Science*, 2008, **319**, 794–797.
73 D. Das, T. Jacobs and L. J. Barbour, *Nat. Mater.*, 2010, **9**, 36–39.
74 E. R. Engel, V. J. Smith, C. X. Bezuidenhout and L. J. Barbour, *Chem. Commun.*, 2014, **50**, 4238–4241.
75 A. Janiak, C. Esterhuysen and L. J. Barbour, *Chem. Commun.*, 2018, **54**, 3727–3730.
76 C. Yang, X. Wang and M. A. Omary, *Angew. Chem., Int. Ed.*, 2009, **48**, 2500–2505.
77 H.-L. Zhou, Y.-B. Zhang, J.-P. Zhang and X.-M. Chen, *Nat. Commun.*, 2015, **6**, 6917.
78 H. Birkedal and D. Schwarzenbach, *Angew. Chem., Int. Ed.*, 2002, **41**, 754–756.
79 A. D. Fortes, E. Suard and K. S. Knight, *Science*, 2011, **331**, 742–746.
80 K. W. Chapman, P. J. Chupas and C. J. Kepert, *J. Am. Chem. Soc.*, 2006, **128**, 7009–7014.
81 A. L. Goodwin, K. W. Chapman and C. J. Kepert, *J. Am. Chem. Soc.*, 2005, **127**, 17980–17981.
82 S. Margadonna, K. Prassides and A. N. Fitch, *J. Am. Chem. Soc.*, 2004, **126**, 15390–15391.
83 Z. Pan, J. Chen, R. Yu, L. Patra, P. Ravindran, A. Sanson, R. Milazzo, A. Carnera, L. Hu, L. Wang, H. Yamamoto, Y. Ren, Q. Huang, Y. Sakai, T. Nishikubo, T. Ogata, X. Fan, Y. Li, G. Li, H. Hojo, M. Azuma and X. Xing, *Chem. Mater.*, 2019, **31**, 1296–1303.
84 A. E. Phillips, A. L. Goodwin, G. J. Halder, P. D. Southon and C. J. Kepert, *Angew. Chem., Int. Ed.*, 2008, **47**, 1396–1399.
85 Y. Wu, A. Kobayashi, G. J. Halder, V. K. Peterson, K. W. Chapman, N. Lock, P. D. Southon and C. J. Kepert, *Angew. Chem., Int. Ed.*, 2008, **47**, 8929–8932.
86 O. V. Dolomanov, L. J. Bourhis, R. J. Gildea, J. A. K. Howard and H. Puschmann, *J. Appl. Crystallogr.*, 2009, **42**, 339–341.
87 G. M. Sheldrick, *Acta Crystallogr., Sect. C: Struct. Chem.*, 2015, **71**, 3–8.
88 C. F. Macrae, I. J. Bruno, J. A. Chisholm, P. R. Edgington, P. McCabe, E. Pidcock, L. Rodriguez-Monge, R. Taylor, J. van de Streek and P. A. Wood, *J. Appl. Crystallogr.*, 2008, **41**, 466–470.
89 M. J. Cliffe and A. L. Goodwin, *J. Appl. Crystallogr.*, 2012, **45**, 1321–1329.

